How does a slender tibia resist buckling? The effect of material, structural and geometric characteristics on the buckling behaviour of the hindleg tibia in the postembryonic development of the stick insect *Carausius morosus*

Maximilian Schmitt[1,2], Thies H. Büscher[1], Stanislav N. Gorb[1] and Hamed Rajabi[*1]

[1]Functional Morphology and Biomechanics, Institute of Zoology, Kiel University, Kiel, Germany
[2]Westphalian Institute for Biomimetics, Westphalian University of Applied Sciences, Bocholt, Germany

* Corresponding author: hrajabi@zoologie.uni-kiel.de; harajabi@hotmail.com

Summary statement

This study provides the first quantitative data on changes in biomechanical properties of cuticle of the hindleg tibia during the entire life of the stick insect *Carausius morosus*.

Abstract

During their lifespan, the long and narrow tibiae of the stick insect *Carausius morosus* (Sinéty, 1901) experience substantial compressive loads. The mechanical load on the tibiae increases as the weight of the insect rises. The increase in the body weight is accompanied by a notable increase in the insect's body size and, accordingly, by an increase in the length of the tibiae. These changes can both raise the risk of buckling of the tibiae. In this study, we track changes in the material and geometric properties of the hindleg tibia of *C. morosus* during growth. The results show that although buckling (either by Euler buckling or local buckling) is the dominant failure mode under compression, the tibia is well capable of maintaining its buckling resistance in each postembryonic developmental stage. This is found to be essentially the result of a compromise between the increasing slenderness of the tibia and its increasing material stiffness. The use of an optimal radius to thickness ratio, a soft resilin-dominated core, and chitin fibres oriented in both longitudinal and circumferential directions are presumably additional strategies preventing buckling of the tibia. This study, providing the first quantitative data on changes in the biomechanical properties of cuticle during the entire life of an insect, is expected to shed more light on the structure-property-function relationship in this complex biological composite.

Keywords: stick insect, buckling, tibia, cuticle, stiffness, slenderness.

1. Introduction

The term "compression-member" is employed in engineering to describe structures which are designed to resist compressive forces (Budynas & Nisbett, 2015). Such structures are widely used in civil and mechanical engineering for load-carrying and supporting purposes. Although structurally very efficient, compression-members have a major disadvantage: When designed slender, they are susceptible to failure by buckling.

Buckling is a complex mechanical phenomenon arising from instability of a structure subjected to compressive stresses. In slender compression-members, buckling takes place spontaneously and far below the strength of the material of which the structure is made (Beer et al., 2006). Hence, it is known to be one of the most catastrophic failure modes (Levy & Salvadori, 1992). This is somewhat reflected in a relatively large factor of safety of engineering structures subjected to axial compression, considered to be about four times higher than that of a similar structure under tension (Grote & Feldhusen, 2011). This higher factor of safety is often achieved by three key strategies: (i) the use of materials with higher Young's moduli, (ii) adding extra material to the cross section and (iii) adjusting the geometric parameters of the member (Clausen, 1851; Keller, 1960; Galambos, 1998).

Buckling, however, is not only limited to metals and traditional engineering materials. Many biological systems have evolved strategies to overcome the problem of failure by buckling (Sakes et al., 2016). An example is the hollow stem of the bamboo plant, known as bamboo culm (Harries et al., 2016). The culm is subdivided into regularly spaced intervals, by so called nodes, recognizable by the presence of external circular ridges. While the hollow structure increases the structural stiffness of the culm for a given weight, the nodes improve its resistance to local buckling (Kappel et al., 2004). The latter is achieved by providing extra reinforcement and reducing the effective length of the culm.

The use of a foam-like infill is another strategy utilized by some biological systems. The foam core, which provides internal support against kinking, can usually be found in plant stems, echidna spines and porcupine quills, all having closed-cell foam-filled cores (Karam & Gibson, 1994). The foams may be additionally stiffened by thin, solid, radially extended ribs (Vincent & Owers, 1986). In some cases, as that of hedgehog spines, the foams may form a honeycomb structure, resulting in a remarkable increase in buckling resistance comparing to an equivalent hollow cylinder (Karam & Gibson, 1994).

In comparison to the above mentioned structural examples, some members of parasitic hymenopteran families (e.g. Aulacidae) (Hedicke, 1939) employ an adaptive behaviour as a buckling prevention mechanism in their long ovipositor (Sakes et al., 2016). Although the ovipositor in this group shows

several morphological adaptations (Vilhelmsen et al., 2001), it is additionally supported by the insects' hindlegs (Sakes et al., 2016). During penetration into a substrate, the ovipositor is held between the legs, reducing its unsupported length.

Similar to many other body parts, insect legs, and in particular their tibiae, experience excessive bending and compressive stresses during their lifespan (Parle et al., 2016a). Taking into account their thin-walled hollow structure, such stresses increase the risk of buckling failure in tibiae, and thus potentially reduce insect survival. Therefore, it is reasonable to expect that insect tibiae are adapted to better resist buckling. Our knowledge about the buckling behaviour of insect tibiae, however, is limited to only a few recent reports (Parle et al., 2016a; b; 2017). Although these studies suggest that tibiae in some insects have adapted to better resist buckling, we are not fully aware of the mechanisms underlying this ability (Parle et al., 2016b). Here, therefore, we utilize a combination of mechanical testing and modern imaging techniques to address these questions experimentally. The well-established model organism in insect locomotion (Graham, 1972; Schütz & Dürr, 2011), sensory physiology (Tichy, 1979), and control (Dean, 1991), the stick insect *Carausius morosus* (Sinéty, 1901), was used in this study. Stick insects (Phasmatodea Jacobson & Bianchi, 1902) in general possess considerably elongated extremities, usually with very long and slender tibiae. It is currently unknown whether, during daily activities, tibiae are in danger of buckling. But, especially in case of a possible drop down from elevated vegetation in which most species dwell (Büscher & Gorb, 2017), they seem to be notably prone to buckling.

Since these stick insects are hemimetabolous, thier tibiae scale up during the lifetime from the first nymphal stage to the adult. We tracked changes in the geometric characteristics, material properties and mechanical behaviour of the hindleg tibia, which is supposed to experience highest forces during the insect locomotion, if compared to the other legs (Pfeiffer et al., 1991). We aim to answer the following questions:

(i)   How do geometric parameters of the tibia, such as length, radius, thickness, slenderness ratio and cross sectional shape change during development?

(ii)   Does the Young's modulus of the tibia cuticle change during insect lifetime?

(iii)   How do the geometry of the tibia and the Young's modulus of its material influence the buckling resistance of the tibia at each postembryonic developmental stage?

(iv)   Which biomechanical strategies do influence the buckling behaviour of the tibia?

2. Materials and methods

    2.1.   Species

The stick insect *C. morosus* has six nymphal stages followed by the adult stage. The stick insects were taken from our laboratory culture and raised separately, in order to precisely track the nymphal stage and notice moulting events. They were fed with fresh blackberry leaves and water ad libitum, and kept under a natural day/night cycle. We always used hindleg tibiae of those specimens which were in the second week after moulting. For this purpose, the insects were first anesthetized with CO_2, and then either right or left hindleg tibia was cut using a sharp razor blade. Afterwards the insects were quarantined until the cut legs have been autotomized thoroughly by the insects, and then returned to the laboratory culture after recovery. All procedures comply with ethical guidelines at Kiel University.

2.2. Mechanical testing

Compression tests were performed using a ZwickiLine uniaxial compression testing machine (Zwick Roell, Ulm, Germany) equipped with a 5 N load cell (Xforce P load cell, Zwick Roell, Ulm, Germany) (figure 1B). The freshly cut hindleg tibiae were placed at their distal end on a 3D-printed sample holder having a 1 mm-deep hole in the middle. The specimens were fixed in the hole using a small drop of hot wax. The proximal end of the specimens was placed in contact with a rough sandpaper adhered to the load cell. This enabled us to more precisely control the straightness of specimens prior to the experiment. Compression tests were always performed at an increasing displacement of 5 mm/min. Force and displacement were continuously recorded by the software testXpert (v 3.5, Zwick Roell, Ulm, Germany) throughout the experiment. We finished each experiment maximum within 15 min after removal of the tibiae from the insects' body. The whole testing process was filmed using a Nikon D5300 digital camera (Nikon corp., Tokyo, Japan) equipped with a macro lens (Canon Macro Lens EF 100 mm, Canon Inc., Tokyo, Japan). Mechanical tests were conducted on ten to seventeen hindleg tibiae at each postembryonic developmental stage (table 1).

We estimated the effective Young's modulus (E) of the tibia cuticle using the following equation:

$$E = \frac{FL}{A\delta} \ ,$$ (1)

where F is the measured force at any point of the linear portion of the force-displacement curve and δ is the corresponding displacement. A and L are the average cross sectional area and length of tested tibiae.

The stress at buckling was calculated by dividing the force at buckling (F_b) by the cross sectional area of specimens at the buckling site:

$$\sigma_b = \frac{F_b}{A}. \tag{2}$$

The cross sectional area at the buckling site was taken as the average cross sectional area of at least three specimens at that region (see section 2.3). The buckling sites were identified from the recorded videos.

When loaded in axial compression, a column-like structure could fail either at a material or a structural level. Failure at the material level is essentially due to fracture or plasticity. In such cases, failure occurs when the stress at any point of the structure exceeds the ultimate compressive strength (σ_{uc}) or the yield strength (σ_y) of the material of which it is made. Failure at a structural level, however, could occur either by Euler or local buckling. The stress required to cause failure by Euler buckling can be theoretically predicted using the following formula (Timoshenko, 1953):

$$\sigma_{Euler} = \frac{\pi^2 EI}{AL_e^2}, \tag{3}$$

where I and L_e are the minimum second moment of area and effective length of the column, respectively. The stress needed to induce local buckling can be estimated by (Timoshenko & Gere, 1961; Rees, 1997):

$$\sigma_{local} = \frac{E}{2\sqrt{3(1-v^2)}} \frac{t}{r}, \tag{4}$$

where t and r are the thickness and outer radius of the column, respectively. v is the Poisson's ratio of the column material, and here it is assumed to be 0.3.

2.3. Micro-computed tomography scanning

Micro-computed tomography (µCT) scanning was used to measure the geometric parameters of the hindleg tibia of the stick insect at all seven postembryonic developmental stages. The tibiae were dried in an ascending ethanol series prior to scanning. All tibiae were scanned using a Skyscan 1172 µCT scanner (Bruker, Kontich, Belgium) with a resolution of 1-3 µm at a peak voltage of 40 kV and a current of 250 µA. The scans were performed on at least three tibiae at each developmental stage.

The obtained data were used to calculate the second moment of area (I), cross sectional area (A), thickness (t) and radius (r) of the specimens. Measurements were performed using BoneJ (Doube et al., 2010) and ImageJ software (v 1.5i, National Institutes of Health, Bethesda, MD).

The slenderness ratio of specimens was calculated by dividing the length (L) to minimum radius of gyration (r_g):

$$SR = \frac{L}{r_g},$$ (5)

where r_g is obtained by

$$r_g = \sqrt{\frac{I}{A}}.$$ (6)

We used the data from µCT scans to measure the area and second moment of area for more than 2000 cross sections of each scanned specimen. The above equation was then used to calculate the radius of gyration of each cross section. The minimum obtained value was taken as the minimum radius of gyration of that specimen. The minimum radius of gyration of specimens at each developmental stage was assumed to be equal to the average of those of at least three tibiae at that stage.

2.4. Scanning electron microscopy

For scanning electron microscopy (SEM), three tibiae at each developmental stage were first air-dried, and then broken into smaller pieces. The fractures were mounted on SEM stubs using carbon Leit-tabs (Plano GmbH, Wetzlar, Germany). They were sputter-coated with a ~10 nm thick gold-palladium layer. The broken sections of the tibiae were imaged using a Hitachi S-4800 scanning electron microscope (Hitachi High-Tech., Tokyo, Japan) at 3 KV accelerating voltage.

2.5. Confocal laser scanning microscopy

Confocal laser scanning microscopy (CLSM) was utilized to obtain an understanding of the material composition of the tibia cuticle. We used the method described by Michels & Gorb (2012) and previously employed by us to demonstrate the presence of the soft and hard cuticle in insect exoskeletons (Rajabi et al., 2015; 2017a; submitted). For this purpose, three freshly cut tibiae at each developmental stage were first washed in distilled water. They were then carefully cut in pieces with ~0.5 mm thickness using a sharp razor blade. The obtained sections were mounted in glycerine between a glass slide and a cover slip.

We used a Zeiss LSM 700 microscope (Carl Zeiss Microscopy, Jena, Germany) to visualize the cross section of the specimens. The microscope was equipped with four stable solid-state lasers (405 nm, 488 nm, 555 nm and 639 nm) and four emission filters (BP420–480, LP490, LP560 and LP640 nm).

2.6. Statistics

Statistical analyses were performed according to the protocol suggested by Nayak & Hazra (2011). Since the obtained data were unpaired and non-parametric, the Kruskal-Wallis *H* test was utilized to compare data sets. The analysis was followed by Dunn's *post hoc* test when appropriate. The values in the text are shown in mean ± standard deviation, if not stated otherwise.

3. Results

Representative force-displacement curves obtained from uniaxial compression tests on the hindleg tibiae of the stick insect *C. morosus* are shown in figure 1A. As seen here, prior to buckling, the tibiae exhibit a linear elastic behaviour. Once buckling takes place, the slope of the force-displacement curve decreases (onset of buckling). The buckling of the tibiae at different postembryonic developmental stages appears to occur in two different modes (shown by black and red dash-lines). The first buckling mode is associated with the sideways bending of the whole sample (black dash-line, onset of Euler buckling). This buckling mode, known as Euler buckling, results in instability of the tibia. In this state, any further loading will cause the formation of a plastic hinge and, finally, the collapse of the specimen. This buckling mode is characteristic of specimens at the last nymphal and adult stages (L6 & Adult). The hindleg tibiae of individuals at the first five nymphal stages (L1-L5), however, buckle in a different way. In these specimens, the instability is initiated by formation of a localized kink (red dash-line, onset of local buckling). The initial local buckling is subsequently followed by out-of-straightness of the tibia. In contrast to Euler buckling, localized buckling results in a sudden reduction of the resistance of the tibia to the applied displacement. Videos S1 and S2 show the onset and evolution of buckling in two tibia specimens at the fifth nymphal stage (L5) and adult stage (Adult), respectively.

Figure 2A shows the critical buckling force of the hindleg tibia at each postembryonic developmental stage. The specimens at the first nymphal stage (L1) have the lowest critical force, 4±2 mN. The force increases from the first (L1) to the fourth nymphal stage (L4), in which it is 39±21 mN. From this stage, the critical force increases again, but at a slightly higher rate until it reaches a maximum value of 127±20 mN, at the adult stage (Adult).

The stress at buckling at each postembryonic developmental stage is given in figure 2B. The stress varies from a minimum value of 11.26 MPa, at the fourth nymphal stage (L4), to a maximum value of 112.67 MPa, at the fifth nymphal stage (L5). The mean stress, in contrast, is found to vary in a rather narrow range from 37.42 MPa, at the adult stage, to 67.33 MPa, at the fifth nymphal stage (L5). According to statistical analysis, however, no significant difference is observed between the stresses at different stages (H=15.62, N=89, P>0.05).

We estimated the stress in the tibia in a simple standing posture by dividing the insect body weight to the sum of the cross sectional area of six tibiae. The stress induced by the body weight at each stage is given in figure 2C. Similar to the stress at buckling, no significant difference could be found between the stresses at the different stages (H=16.58, N=89, P>0.05).

The effective Young's modulus is used as a measure of the stiffness of the tibia cuticle (figure 2D). It can be seen that the effective Young's modulus slightly decreases from 1.2±0.3 GPa, at the first nymphal stage (L1), to 0.8±0.3 GPa, at the second nymphal stage (L2). However, the statistical analysis shows no significant difference between the moduli at these two stages (N=24, P>0.05). No significant difference can also be found when comparing the effective Young's modulus of specimens at the sixth nymphal stage (L6, 4.5±0.6 GPa) and the adult stage (Adult, 3.7±0.8 GPa) (N=26, P>0.05). Except the slight differences between the aforementioned groups, the general trend in the effective Young's modulus is an upward increase as the insect grows.

Figure 3 represents the geometric parameters of the hindleg tibia at each postembryonic developmental stage. A gradual change can be observed in the length and cross sectional shape of the tibia during the insect growth (figure 3E). The data obtained from μCT analysis (available on request) were used to calculate the slenderness ratio of the tibia, presented in figure 3A. When comparing the slenderness ratios of the tibia at different stages, statistical analysis reveals no significant difference between them at the first five nymphal stages (L1-L5) (N=67, P>0.05). We also found no significant difference between the slenderness ratios at the last nymphal stage (L6) and the adult stage (Adult) (N=26, P>0.05). However, statistics show a significant difference between the slenderness ratios of the tibiae in the two mentioned groups (i.e., the first five nymphal stages, L1-L5, and the last two living stages, L6 & Adult) (H=58.23, N=93, P<0.05).

The radius to thickness (r/t) ratio of the tibia, shown in figure 3B, is found to increase from 6.84±0.67, at the first nymphal stage (L1), to 13.13±1.21, at the fifth nymphal stage (L5). From the latter stage (L5) to the sixth nymphal stage (L6), the r/t ratio suddenly drops to 4.32±0.37, but it remains almost constant from the sixth nymphal stage (L6) to the adult stage (Adult) (N=16, P>0.05).

The results of CLSM revealed the presence of two distinguishable layers with different autofluorescence characteristics in the hindleg tibia cuticle (figure 4D,E). According to Michels & Gorb (2012), the blue autofluorescence of the inner layer indicates the high proportion of resilin, the pliant protein. The outer layer, in contrast, shows a strong green autofluorescence, which suggests that this layer mainly consists of sclerotized chitinous material. Figure 3C shows the area of the hard sclerotized and soft resilin-dominated cuticle as a fraction of total area obtained from measurements on tibia cross sections. Using these data, we calculated the area ratio of the hard to soft cuticle at all stages (figure 3D). Interestingly, the obtained data seem to follow the same trend as that observed in the effective Young's modulus. The area ratio of the hard to soft cuticle slightly decreases from 0.39±0.03, at the first nymphal stage (L1), to 0.34±0.02, at the second nymphal stage (L2). After this, the area ratio continuously increases until it reaches a maximum value of 0.65±0.01, at the sixth nymphal stage (L6). The area ratio of the hard to soft cuticle at the adult stage (Adult, 0.57±0.03) is found to be slightly lower than that measured in the former stage (L6).

Figure 4B,C,F shows representative SEM images of the hindleg tibia cuticle. The obtained images suggest that the tibia cuticle consists of up to five main layers: (i) epicuticle, (ii) outer exocuticle, (iii) mesocuticle, (iv) inner exocuticle and (v) endocuticle. Epicuticle is the outermost layer which is usually very thin with a thickness reaching up to 0.5 µm in adult individuals. The epicuticle covers a very dense exocuticular layer with a lamellar organization. The thickness of this layer in adult specimens is measured to be 1.0-2.8 µm. Below the exocuticle, there is a less dense layer, most likely a mesocuticle, with a thickness ranging from 2.0 µm to 3.6 µm in adult individuals. Due to its less-organized structure, it is not possible to unambiguously determine the arrangement of chitin microfibers in this layer. We found another exocuticle layer just beneath the mesocuticle. Although it is less dense than the outer exocuticle, they both seem to have a similar layered structure. The inner exocuticle can reach a thickness of up to 2 µm in the adult stick insects. The innermost layer in the cuticle microstructure is a less dense endocuticle, consisting of alternating thin helicoidal and thicker unidirectional layers. The unidirectional layers within the endocuticle, in some regions, have the same orientation, and together with helicoidal layers they build a so-called locust-like layering (Neville & Luke, 1969) (figure 4B). In some other regions, however, they

change the orientation by 90°, resulting in formation of a pseudo-orthogonal layering (Neville & Luke, 1969) (figure 4F). The endocuticle, with a thickness of 8-16 µm in adult individuals, is the thickest layer in the tibia cuticle. Although we are able to confirm the presence of the aforementioned layers in tibiae at all postembryonic developmental stages, their thickness is found to be very variable. The thickness of each certain layer is also seen to be highly dependent on the measurement point on the tibia, even in one single individual.

The measured mechanical and geometric characteristics of the tibia during the development of the stick insect *C. morosus* are summarized in table 1.

4. Discussion

A variety of biological factors may influence the mechanical behaviour of tibiae of the stick insect *C. morosus*. An example is the increase in the body size (figure S1B), which has an inevitable impact on the length of the tibia (figures 3E & S1C). The increase in the body size further results in an increase in the body mass (figure S1A) and, consequently, raises the force acting on each tibia. Although one may expect that the added body mass at each postembryonic developmental stage increases the mechanical stress in the tibiae, a simple estimation suggests that this is not the case (figure 2C). Indeed, we found no significant difference between the stresses applied to the tibiae by the weight of the insect at different developmental stages. This may be a major reason why the buckling resistance of the hindleg tibia also remains constant during the insect growth (figure 2B).

A remarkable difference, however, was observed between the values of the stress at buckling and the stress imposed on the hindleg tibia by the body weight (figure 2B,D). Comparison of the two stresses at the adult stage, for instance, suggests that the tibia possesses a large factor of safety of 127.2±23.2 in standing posture. Using kinematic data from the literature, we additionally determined the factor of safety of the tibia when subject to compressive stresses during daily activities. The data from ground reaction force measurements on freely walking adult stick insects showed that compressive forces in the insect hindlegs can reach a peak value of 9.6 mN (Dallmann et al., 2016). Assuming the entire force to be transmitted to the tibia, this results in a factor of safety of 13.7±2.2 for the tibia when walking. This is about twice the maximum factor of safety measured for the tibia of other arthropods, ranged from 1.7 to 7 (Parle et al., 2016a). This finding, therefore, raises the question of why the tibia needs such a high load-carrying capacity.

A recent study reported frequent intentional drops or accidental falls of the wingless stick insect *Extatosoma tiaratum*, while climbing vegetation (Zeng et al., 2015). This behaviour, which may serve as a defence reaction, is likely to be also valid for the wingless species *C. morosus*. Immediately after falling from height, the stick insects are able to reorientate and stabilize their body during the plunge (Zeng et al., 2017), and land on their tarsi (own observation). However, landing on the tarsi may induce much higher stresses in the tibiae than those applied in normal standing posture (Heitler, 1977). Although further investigations are needed, this may explain the large factor of safety considered in the design of the hindleg tibia.

It is well-known that the resistance of a structure to buckling is essentially influenced by its geometric characteristics, in particular slenderness, and the stiffness of the material of which the structure is made (Cedolin, 2010). The increase of the slenderness ratio, leading to a reduced buckling resistance, seems to be inevitable by the insect growth. In the case of the stick insect *C. morosus*, this is reflected in the significant increase of the slenderness ratio of the tibia from the first five nymphal stages (L1-L5) to the last two living stages (L6 & Adult) (figure 3A). On the other hand, except the slight decreases in the effective Young's modulus, the development of the stick insect is accompanied by a significant increase in the stiffness of its tibia cuticle (figure 2D). The increase in the effective Young's modulus appears to compensate the negative effect of the increasing slenderness, enabling the tibia to retain its buckling resistance during the insect growth (figure 2B).

The change of the effective Young's modulus during the insect postembryonic development was found to follow the same trend as that of the area proportion of the hard sclerotized to soft resilin-dominated cuticle (figures 2D and 3D). Taking into account the predominant role of the sclerotized cuticle in stiffening insect cuticle (Hepburn, 1985; Rajabi et al., 2017b), the similar trend between these two parameters appears to be very reasonable. The slight decrease in the effective Young's modulus from the sixth nymphal stage (L6) to the adult stage (figure 2D) can also be explained by the presence of a lower area proportion of the hard to soft cuticle at the latter (Adult) compared to the former (L6) (figure 3C,D). Taking into account the remarkably longer life period of *C. morosus* at the adult stage than at all nymphal stages together (Roth, 1917), it is reasonable to hypothesize that the deposition of the resilin-dominated endocuticle at the adult stage is also more prolonged.

We were able to distinguish two distinctly different force-displacement curves in the results from the uniaxial compression tests on tibia specimens. While the specimens at the first five nymphal stages (L1-L5) suddenly lose their load-carrying capacity after buckling, those at the last nymphal and adult stages (L6 & Adult) show a gradual reduction in their ability to support the external load (red and black dash-lines in figure 1A, respectively). This difference appears to be essentially the result of the occurrence of two different buckling modes in these two groups of specimens (i.e., local buckling and Euler buckling, respectively). This finding is also consistent with the observation of the considerably lower r/t ratio of the tibiae at the sixth nymphal and adult stage (L6 & Adult), if compared to the other living stages (L1-L5) (figure 3B). Although the higher r/t ratio of the tibiae in the latter group (i.e., L1-L5) causes them to become more resistant to Euler buckling, this subsequently makes them more prone to local buckling.

Here, we adapted the method suggested by Taylor & Dirks (2012) to find the optimum value of the r/t ratio of the hingleg tibia at each postembryonic developmental stage. This optimum ratio should provide the highest load-carrying capacity for a given weight. As stated, the failure of the tibia under compression is essentially the result of either Euler or local buckling. The graphs of these two buckling modes are plotted as a function of r/t for adult stick insects (blue and grey dash-line in figure 5A). The buckling stress, given by the Euler curve, increases with the increase of the r/t ratio. In contrast, the stress at buckling predicted by the local buckling curve decreases as the r/t ratio increases. The optimum r/t is reached where the two curves intersect. For the tibia of adult specimens, this optimum value occurs at a point where the r/t ratio is equal to 5.72. As seen in figure 5A, the experimentally measured values of r/t ratio, 4-4.46 (black ellipse), are rather close to the theoretically predicted optimum value. Figure 5B compares the experimental r/t values with those calculated theoretically at each postembryonic developmental stage. A good agreement can be found between the two sets of data at all stages, except at the fifth nymphal stage (L5). Our analysis, in general, suggests the presence of a biomechanical adaptation in the hindleg tibia towards an optimum r/t ratio to reduce the probability of failure by buckling. The optimization of the r/t ratio has already been employed in the design of steel circular hollow tubes used in wind turbine towers to control and improve their buckling behaviour (Guo et al., 2013).

As seen in figure 5B, the experimental r/t ratios of tibiae at the first five nymphal stages (L1-L5) are higher than the theoretically predicted optimum values. In contrast, the r/t ratios obtained from measurements on the tibiae at the sixth nymphal and adult stages (L6 & Adult) are lower than the optimum ones. This finding highlights the dependency of the failure mode to the r/t ratio at each stage and further supports our observation that the buckling mode changes by the insect growth.

In the CLSM images, we were able to observe the presence of a material gradient along the thickness of the tibia cuticle (figure 4D,E). The soft resilin-dominated core of the tibia in addition to toughening the whole structure, can improve its resistance to buckling (Karam & Gibson, 1995; Suresh, 2001). The hard sclerotized coverage, in contrast, enhances the stability of the tibia and protects it against mechanical damage (Rajabi et al., 2016). In many regions, interestingly, it is possible to identify a clear border between the hard and soft cuticle layers (figure 4E). This observation confirms our previous finding that a realistic model of insect cuticle, in addition to consideration of a material gradient, should take the discontinuity at the interface of layers into account (Rajabi et al., 2017b). Such a material discontinuity in the insect cuticle may be a biomechanical strategy to avoid the propagation of an already existing crack from one to another layer.

Natural fibre-reinforced composites, such as the tibia cuticle, are well-known for their light weight, high structural integrity, reasonable stiffness, strength and toughness (Mayer & Sarikaya, 2002; Dirks & Taylor, 2012; Keogh et al., 2015). However, the behaviour of such composites under loading is also influenced by their fibre orientation (Laranjeira et al., 2010; Martinie & Roussel, 2011). It has previously been reported that hollow cylinders with fibres oriented in the axial direction have an optimum bending strength (compared to cylinders with fibres at a certain angle). In contrast, those reinforced with fibres in the circumferential direction result in an optimum compression resistance (Li et al., 2006). In the tibia cuticle, we could demonstrate the presence of both mentioned fibre orientations (figure 4F). During the insect lifetime, the tibia experiences a combination of bending and compression. Therefore, it is reasonable to expect that the cuticle in this body part is adapted to resist both loading conditions by aligning fibres in the two mentioned orientations.

Comparison of our results with those of previous measurements on tibiae of the adult stick insects loaded in bending (Parle et al., 2016b) indicates that the bending stiffness of the tibia cuticle is larger than its stiffness in compression (5.5±4.13 GPa and 3.65±0.79 GPa, respectively). The difference between the measured properties is even more striking when comparing the strength of the tibia in bending and compression, found to be 116.0±66.1 MPa and 37.4±15.9 MPa, respectively. This suggests that, although

compression is a typical loading condition for the tibia especially when an insect is standing upright, bending stresses in the leg during daily activities may exceed those caused by compression. Future studies are planned to assess macro- and micro-morphological differences between fore-, mid- and hindlegs of the stick insect *C. morosus* and to evaluate their potential influence on the buckling resistance of each leg under combined bending and compression.

5. Conclusions

In this study, we tracked changes in the material, structural and geometric properties of the hindleg tibia of the stick insect *C. morosus* at all postembryonic developmental stages. We aimed to understand how the observed changes can influence the load-carrying capacity of the tibia under compression. Based on the obtained data, the following conclusions can be drawn:

(i)   Although the geometric characteristics of the hindleg tibia remarkably change during growth, the tibia is able to maintain its resistance against buckling. This is found to be the result of a compromise between the increasing slenderness of the tibia and its increasing stiffness.

(ii)   The failure of the tibia under compression is found to mainly occur in two different buckling modes: local buckling, at the first five nymphal stages, and Euler buckling, at the sixth nymphal and the adult stage.

(iii)   The occurrence of any of the mentioned buckling modes at each developmental stage is likely to be influenced by the ratio of radius to thickness (r/t) of the tibia at that stage. This ratio at most developmental stages is close to an optimum value, representing a good capability to resist both Euler and local buckling.

(iv)   The presence of a soft, resilin-dominated endocuticle with fibres orientated in both longitudinal and circumferential directions is likely to be a biomechanical adaptation that provides the tibia with an enhanced buckling resistance.

Authors' contributions

HR and SNG designed the study; HR and THB coordinated the study; MS performed the experiments; MS and HR analysed the data and wrote the manuscript; all the authors discussed the results, reviewed the manuscript and gave the final approval for publication.

References

Beer, F.P., Johnston, R., Dewolf, J. & Mazurek, D. (2006). Mechanics of materials. New York: McGraw-Hill.

Budynas, R. G., & Nisbett, J. K. (2015). Shigley's mechanical engineering design (10th ed.). New York: McGraw-Hill.

Büscher, T.H. & Gorb, S.N. (2017). Subdivision of the neotropical Prisopodinae Brunner von Wattenwyl, 1893 based on features of tarsal attachment pads (Insecta, Phasmatodea). ZooKeys, 645, 1-11.

Cedolin, L. (2010). Stability of Structures: Elastic, Inelastic, Fracture and Damage Theories. Singapore: World Scientific.

Clausen, T. (1851). Über die Form architektonischer Säulen. Bulletin de la Classe physico-mathématique de l'Académie impériale des sciences de Saint-Pétersbourg, 9, 368-379.

Dallmann, C. J., Dürr, V., & Schmitz, J. (2016). Joint torques in a freely walking insect reveal distinct functions of leg joints in propulsion and posture control. Proceedings of the Royal Society B, 283: 20151708.

Dean, J. (1991). Effect of load on leg movement and step coordination of the stick insect *Carausius morosus*. Journal of Experimental Biology, 159(1), 449-471.

Dirks, J.H. & Taylor, D. (2012). Fracture toughness of locust cuticle. Journal of Experimental Biology, 215(9), 1502-1508.

Doube, M., Kłosowski, M.M., Arganda-Carreras, I., Cordelières, F.P., Dougherty, R.P., Jackson, J.S., Schmid, B., Hutchinson, J.R. & Shefelbine, S.J. (2010). BoneJ: free and extensible bone image analysis in ImageJ. Bone, 47(6), 1076-1079.

Galambos, T.V. (ed.). (1998). Guide to stability design criteria for metal structures. New York: John Wiley & Sons.

Graham, D. (1972). A behavioural analysis of the temporal organisation of walking movements in the 1st instar and adult stick insect (*Carausius morosus*). Journal of Comparative Physiology A: Neuroethology, Sensory, Neural, and Behavioral Physiology, 81(1), 23-52.

Grote, K.-H. & Feldhusen, J. (2011). Dubbel: Taschenbuch für den technischen Maschinenbau. Heidelberg: Springer.

Guo, L., Yang, S. & Jiao, H. (2013). Behavior of thin-walled circular hollow section tubes subjected to bending. Thin-Walled Structures, 73, 281–289.

Harries, K.A., Bumstead, J., Richard, M. & Trujillo, D. (2016). Geometric and material effects on bamboo buckling behaviour. Proceedings of the Institution of Civil Engineers-Structures and Buildings, 170(4), 236-249.

Heitler, W.J. (1977). The locust jump: III. Structural specializations of the metathoracic tibiae. Journal of Experimental Biology, 67(1), 29-36.

Hepburn, H. R. (1985). The integument. In: Fundamentals of Insect Physiology (M.S. Blum ed.), 139-183.

Kappel, R., Mattheck, C., Bethge, K., & Tesari, I. (2004). Bamboo as a composite structure and its mechanical failure behaviour. WIT Transactions on Ecology and the Environment, 73, 285-293.

Karam, G.N. & Gibson, L.J. (1994). Biomimicking of animal quills and plant stems: natural cylindrical shells with foam cores. Material Science and Engineering: C, 2, 113–132.

Karam, G.N. & Gibson, L.J. (1995). Elastic buckling of cylindrical shells with elastic cores - II. Experiments. International Journal of Solids and Structures, 32(8/9), 1285-1306.

Keller, J.B. (1960). The shape of the strongest column. Archive for Rational Mechanics and Analysis, 5(1), 275-285.

Keogh, L., O'Hanlon, P., O'Reilly, P. & Taylor, D. (2015). Fatigue in bamboo. International Journal of Fatigue, 75, 51-56.

Laranjeira, F., Aguado, A. & Molins, C. (2010). Predicting the pullout response of inclined straight steel fibers. Materials and Structures, 43(6), 875-895.

Levy, M. and Salvadori, M. (1992). Why buildings fall down - How structures fail. New York: W.W. Norton & Company.

Li, G., Maricherla, D., Singh, K., Pang, S.S. & John, M. (2006). Effect of fiber orientation on the structural behavior of FRP wrapped concrete cylinders. Composite Structures, 74(4), 475-483.

Martinie, L. & Roussel, N. (2011). Simple tools for fiber orientation prediction in industrial practice. Cement and Concrete Research, 41(10), 993-1000.

Mayer, G. & Sarikaya, M. (2002). Rigid biological composite materials: structural examples for biomimetic design. Experimental Mechanics, 42(4), 395-403.

Michels, J. & Gorb, S.N. (2012). Detailed three-dimensional visualization of resilin in the exoskeleton of arthropods using confocal laser scanning microscopy. Journal of Microscopy, 245(1), 1-16.

Nayak, B.K. & Hazra, A. (2011). How to choose the right statistical test? Indian Journal of Ophthalmology, 59(2), 85.

Neville, A.C. & Luke, B.M. (1969). A two-system model for chitin-protein complexes in insect cuticles. Tissue and Cell, 1(4), 689-707.

Parle, E. & Taylor, D. (2017). The effect of aging on the mechanical behaviour of cuticle in the locust *Schistocerca gregaria.* Journal of the Mechanical Behavior of Biomedical Materials, 68, 247-251.

Parle, E., Larmon, H., & Taylor, D. (2016a). Biomechanical factors in the adaptations of insect tibia cuticle. PloS One, 11(8), e0159262.

Parle, E., Herbaj, S., Larmon, H. & Taylor, D. (2016b). Buckling failures in insect exoskeletons. Bioinspiration & Biomimetics, 11(1), 016003.

Pfeiffer, F., Weidemann, H.-J. & Danowski, P. (1991). Dynamics of the walking stick insect. IEEE Control Systems, 11(2), 9-13.

Rajabi, H., Stamm, K., Appel, E., & Gorb, S. N. (submitted). Micro-morphological adaptations of the wing nodus to flight behaviour in four dragonfly species from the family Libellulidae (Odonata: Anisoptera).

Rajabi, H., Ghoroubi, N., Stamm, K., Appel, E., & Gorb, S. N. (2017a). Dragonfly wing nodus: a one-way hinge contributing to the asymmetric wing deformation. Acta Biomaterialia, 60, 330-338.

Rajabi, H., Jafarpour, M., Darvizeh, A., Dirks, J.H. & Gorb, S.N. (2017b). Stiffness distribution in insect cuticle: a continuous or a discontinuous profile? Journal of the Royal Society Interface, 14(132), 20170310.

Rajabi, H., Shafiei, A., Darvizeh, A., Dirks, J.H., Appel, E., & Gorb, S.N. (2016). Effect of microstructure on the mechanical and damping behaviour of dragonfly wing veins. Journal of the Royal Society Open Science, 3(2), 160006.

Rajabi, H., Ghoroubi, N., Darvizeh, A., Dirks, J. H., Appel, E., & Gorb, S. N. (2015). A comparative study of the effects of vein-joints on the mechanical behaviour of insect wings: I. Single joints. Bioinspiration & Biomimetics, 10(5), 056003.

Rees, D.W.A. (1997). Basic solid mechanics. London: Macmillan.

Roth, H.L. (1917). Observations on the growth and habits of the stick insect. Transactions of the Royal Entomological Society of London, 64, 345-386.

Sakes, A., Dodou, D. & Breedveld, P. (2016). Buckling prevention strategies in nature as inspiration for improving percutaneous instruments: A review. Bioinspiration & Biomimetics, 11(2), 021001.

Schütz, C., & Dürr, V. (2011). Active tactile exploration for adaptive locomotion in the stick insect. Journal of the Royal Society Proceedings B, 366(1581), 2996-3005.

Suresh, S. (2001). Graded materials for resistance to contact deformation and damage. Science, 292, 2247–2251.

Taylor, D. & Dirks, J.H. (2012). Shape optimization in exoskeletons and endoskeletons: A biomechanics analysis. Journal of the Royal Society Interface, 9(77), 3480–3489.

Tichy, H. (1979). Hygro-and thermoreceptive triad in antennal sensillum of the stick insect, *Carausius morosus*. Journal of Comparative Physiology A: Neuroethology, Sensory, Neural, and Behavioral

Physiology, 132(2), 149-152.

Timoshenko, S.P. (1953). History of strength of materials: with a brief account of the history of theory of elasticity and theory of structures. New York: McGraw-Hill.

Timoshenko, S., & Gere, J.M. (1961). Theory of elastic stability (2nd ed.). New York: McGraw-Hill.

Vilhelmsen, L., Isidoro, N., Romani, R., Basibuyuk, H.H., & Quicke, D.L. (2001). Host location and oviposition in a basal group of parasitic wasps: The subgenual organ, ovipositor apparatus and associated structures in the Orussidae (Hymenoptera, Insecta). Zoomorphology, 121(2), 63-84.

Vincent, J.F., & Owers, P. (1986). Mechanical design of hedgehog spines and porcupine quills. Journal of Zoology, 210(1), 55-75.

Zeng, Y., Lin, Y., Abundo, A., & Dudley, R. (2015). Visual ecology of directed aerial descent in first-instar nymphs of the stick insect *Extatosoma tiaratum*. Journal of Experimental Biology, 218(14), 2305-2314.

Zeng, Y., Lam, K., Chen, Y., Gong, M., Xu, Z., & Dudley, R. (2017). Biomechanics of aerial righting in wingless larval stick insects. Interface Focus, 7, 20160075.
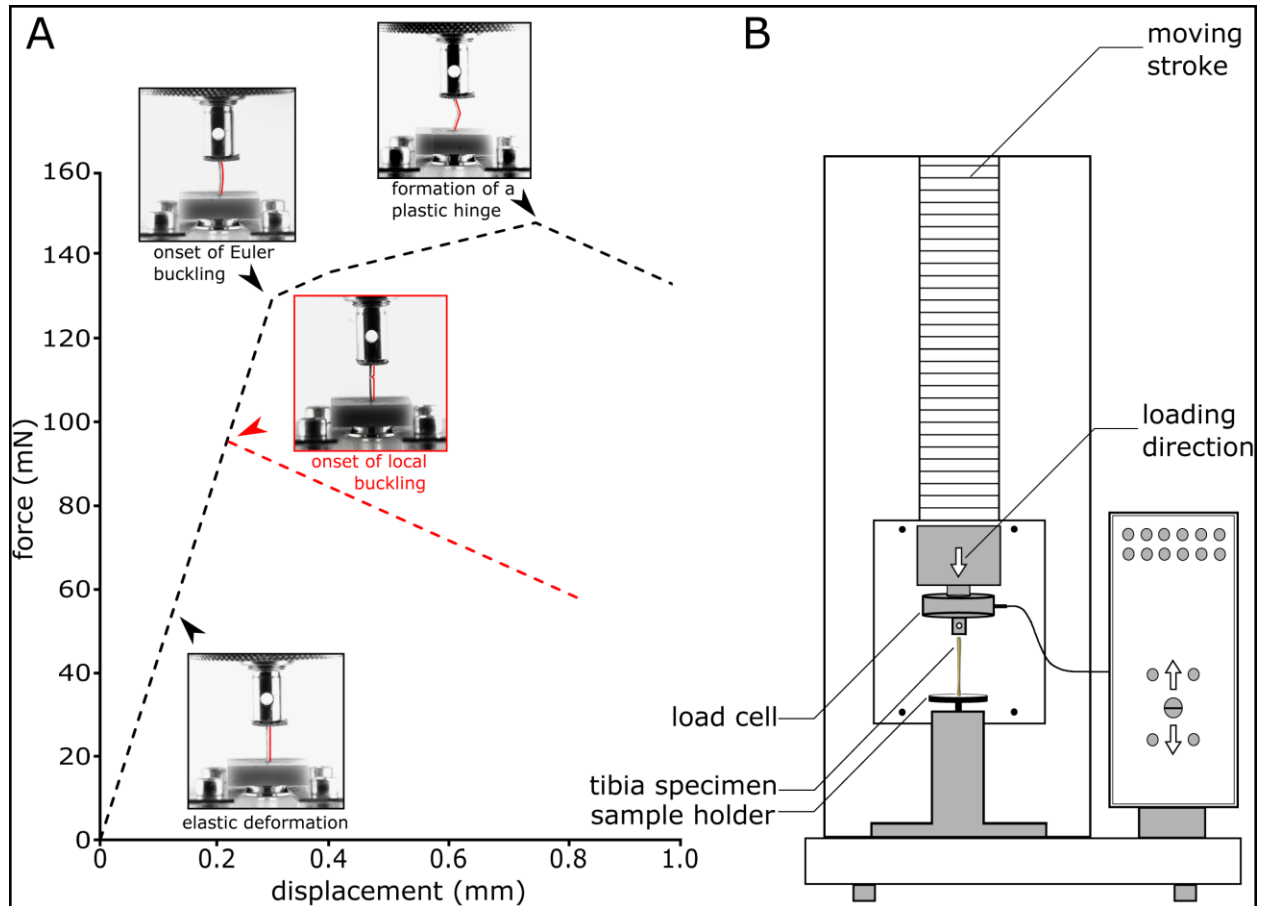
Figures

Figure 1: Uniaxial compression tests on the hindleg tibia of the stick insect *C. morosus*. (A) Representative force-displacement curves of specimens at the first five nymphal stages (L1-L5, red dash-line) and those at the last nymphal and the adult stage (L6 and Adult, black dash-line). (B) Schematic diagram of the compression testing machine. Tibia specimens were fixed on a 3D-printed sample holder and subjected to a displacement-controlled compressive load.
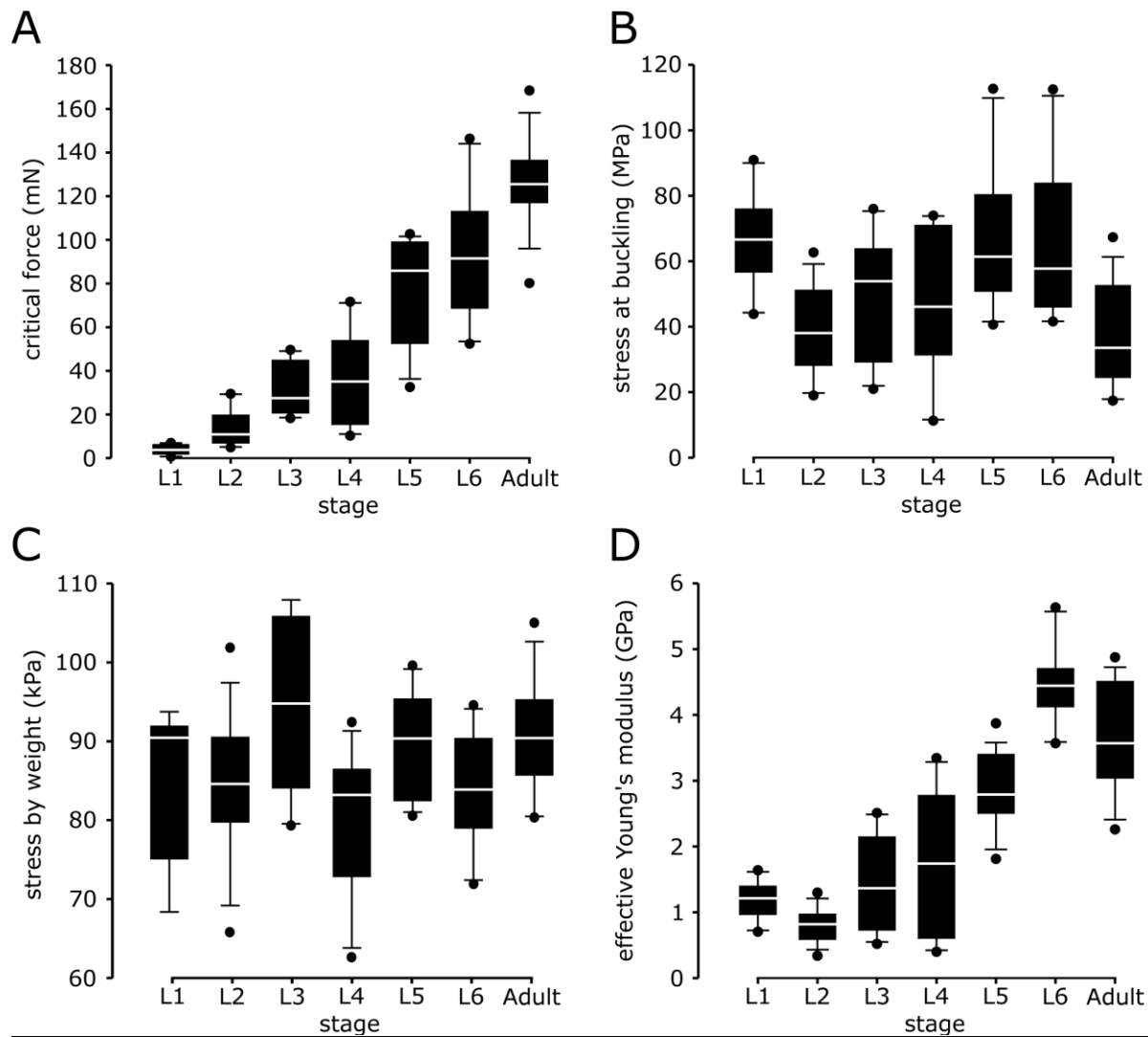
Figure 2: Data obtained from uniaxial compression tests on the hindleg tibia at all postembryonic developmental stages. (A) Critical buckling force increases in the course of the insect development. (B) Stress at buckling of the tibia. According to statistical analysis, there is no significant difference between the stresses at different developmental stages. (C) Stress acting on the tibia due to the insect body weight was also found to remain almost constant during the insect growth. (D) Effective Young's modulus of the tibia cuticle. The general trend is an increase in the effective Young's modulus with the development of the insect. The borders of the boxes indicate the 25th and 75th percentiles, a line within them marks the median, and the whiskers (error bars) define the 10th and 90th percentiles.
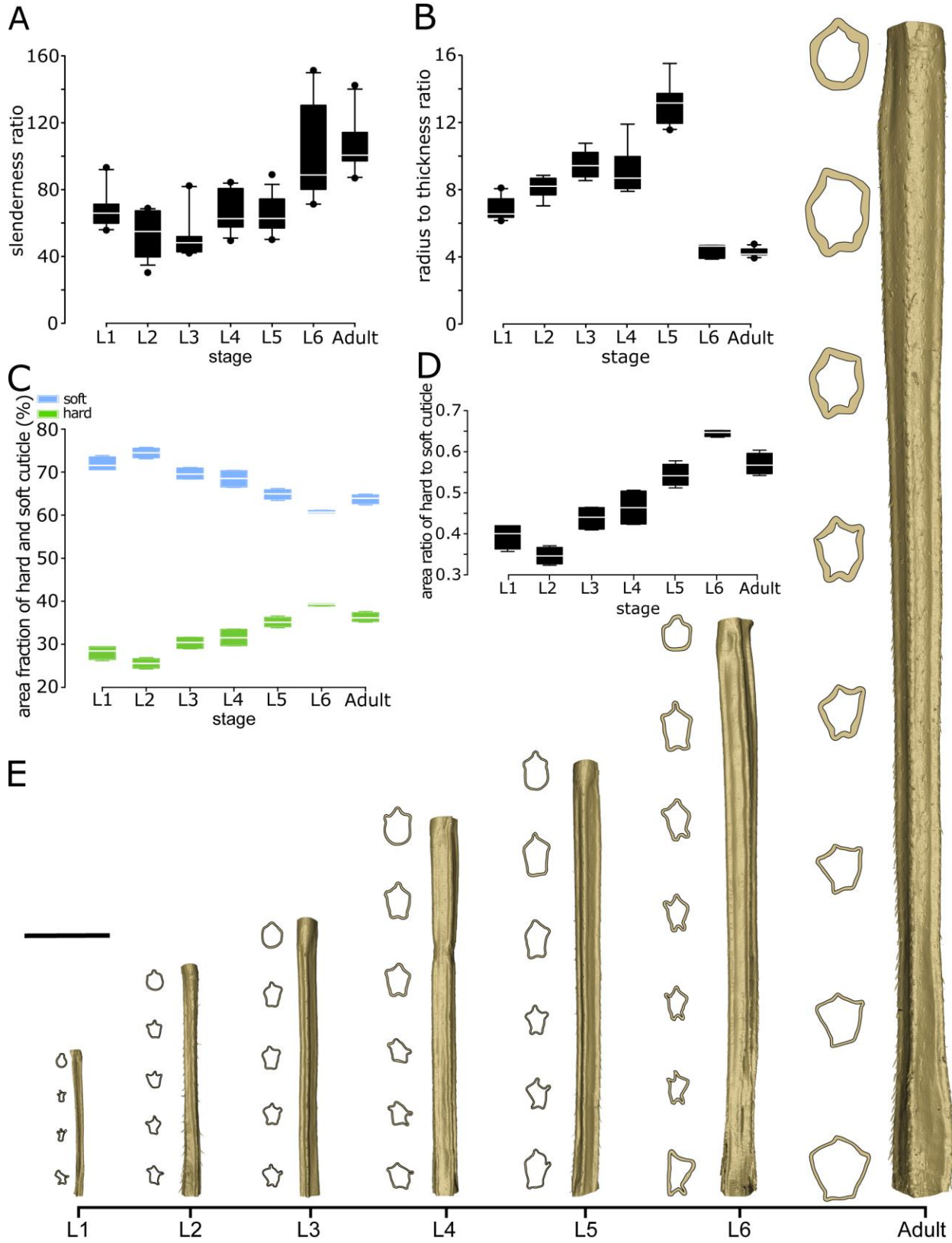
Figure 3: Data from the geometric analysis of the hindleg tibia at all postembryonic developmental stages. (A) Slenderness ratio of the tibia. Although it remains almost constant at the first five nymphal stages (L1-L5), a significant increase is observed in the slenderness from the fifth (L5) to the sixth (L6) nymphal and the adult stage. (B) Ratio of the radius to thickness of the hindleg tibia at each developmental stage. (C) Area of the hard, sclerotized cuticle (green boxes) and soft, resilin-dominated cuticle (blue boxes) as a fraction of the total cross sectional area. (D) Area ratio of the hard to soft cuticle. It appears to follow the same trend as the Young's modulus. (E) Three-dimensionally (3D) reconstructed models of the hindleg tibia at all developmental stages. The cross section of the tibia in several parts is shown beside each model. A gradual change can be seen in the length and cross sectional shape of the tibia during growth. The borders of the boxes indicate the 25th and 75th percentiles, a line within them marks the median, and the whiskers (error bars) define the 10th and 90th percentiles. Scale bar: 1 mm.
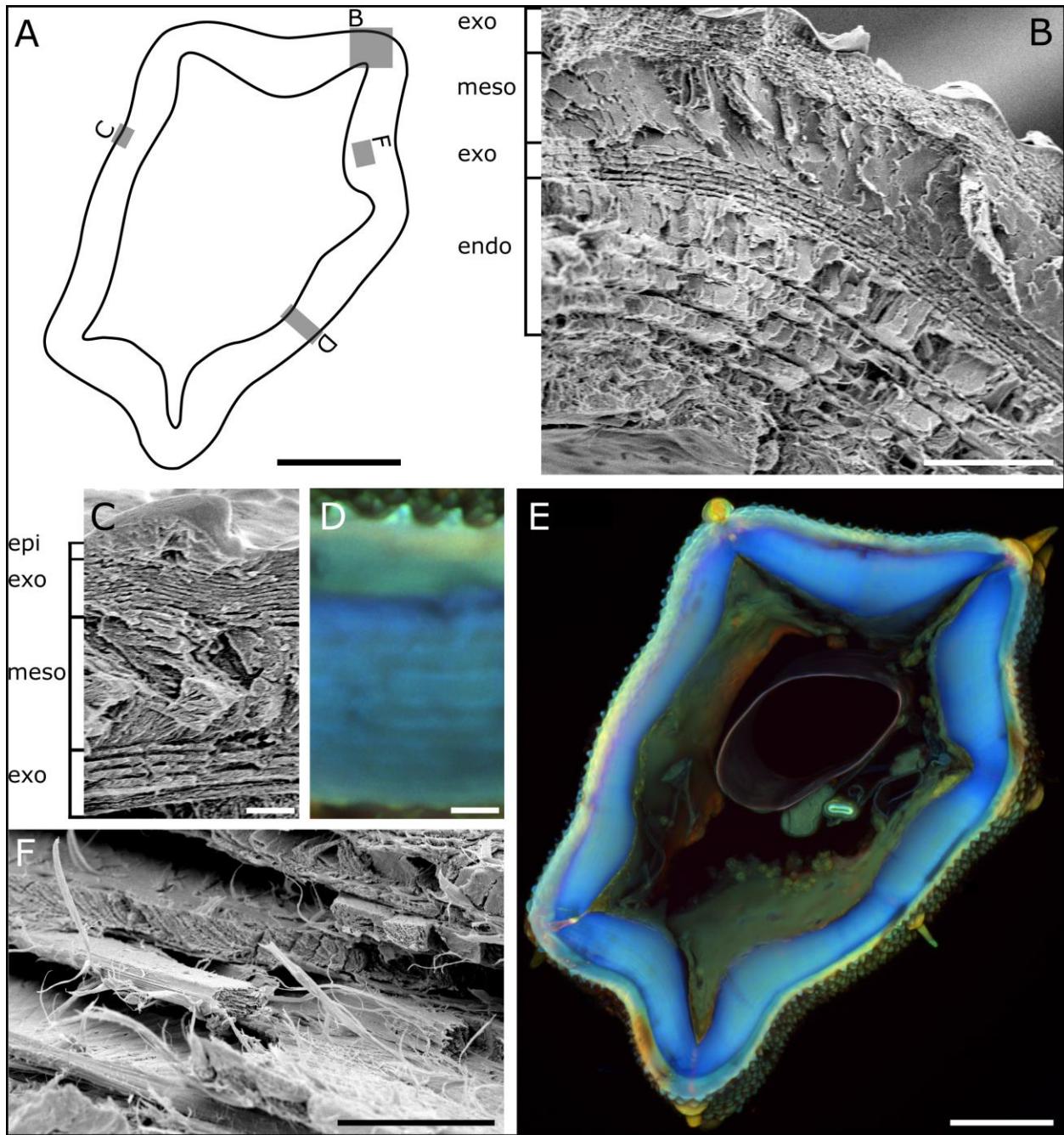
Figure 4: Microstructure and material composition of the hindleg tibia cuticle. (A) Scheme of a tibia cross section showing the approximate position of each given image. (B) SEM image showing the outer exocuticle, mesocuticle, inner exocuticle and endocuticle in a cross section of a specimen at the fifth nymphal stage (L5). (C) SEM image illustrating the lamellar microstructure of the outer and inner exocuticle and the unorganized mesocuticle in a cross section of the tibia at the fifth nymphal stage (L5). The thin epicuticle layer covering the tibia is also visible in this image. (D) CLSM image of the cross section of an adult specimen showing the presence of a material gradient along the thickness of the tibia.

(E) CLSM image of the whole cross section of an adult specimen showing the hard sclerotized and the soft resilin-dominated cuticle in green and blue colours, respectively. (F) A SEM image showing the perpendicularly arranged chitin fibres within the endocuticle of a specimen at the adult stage. Scale bars: 100 µm (A), 10 µm (B), 2 µm (C), 10 µm (D), 100 µm (E) and 5 µm (F).
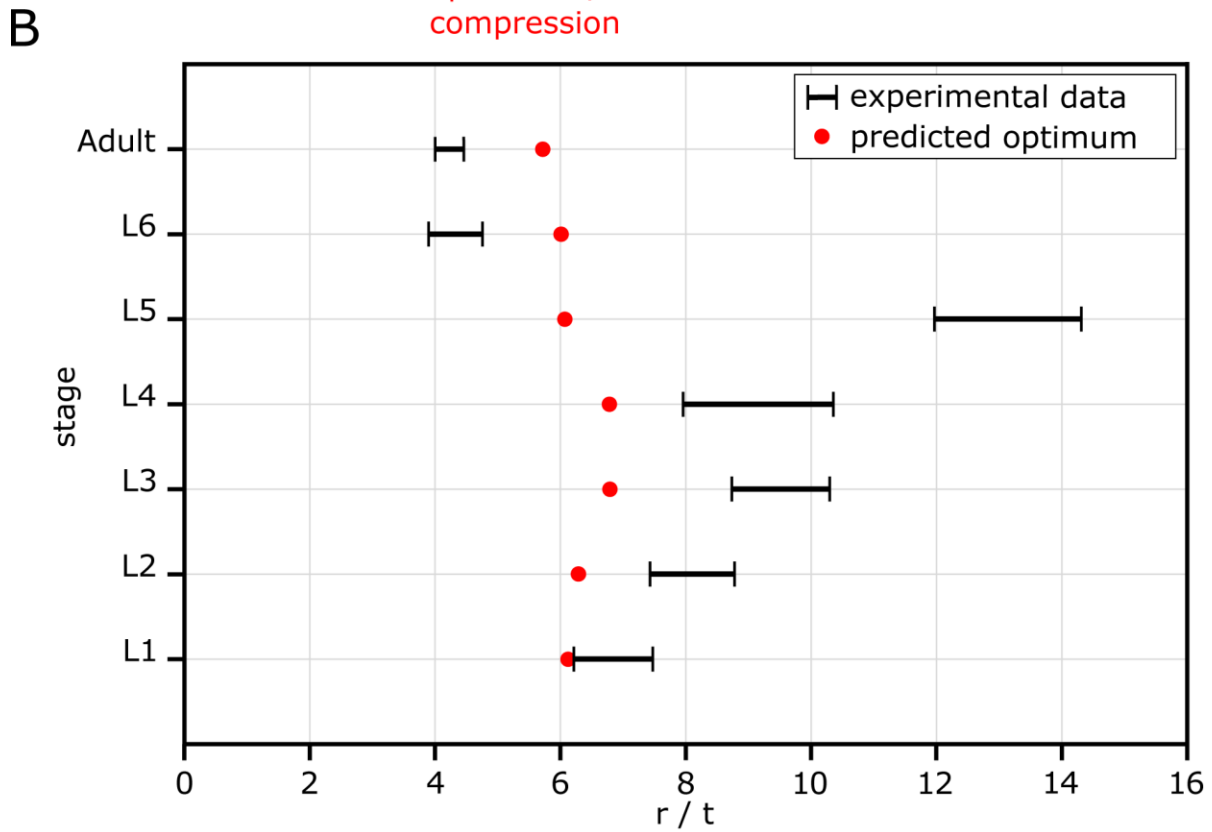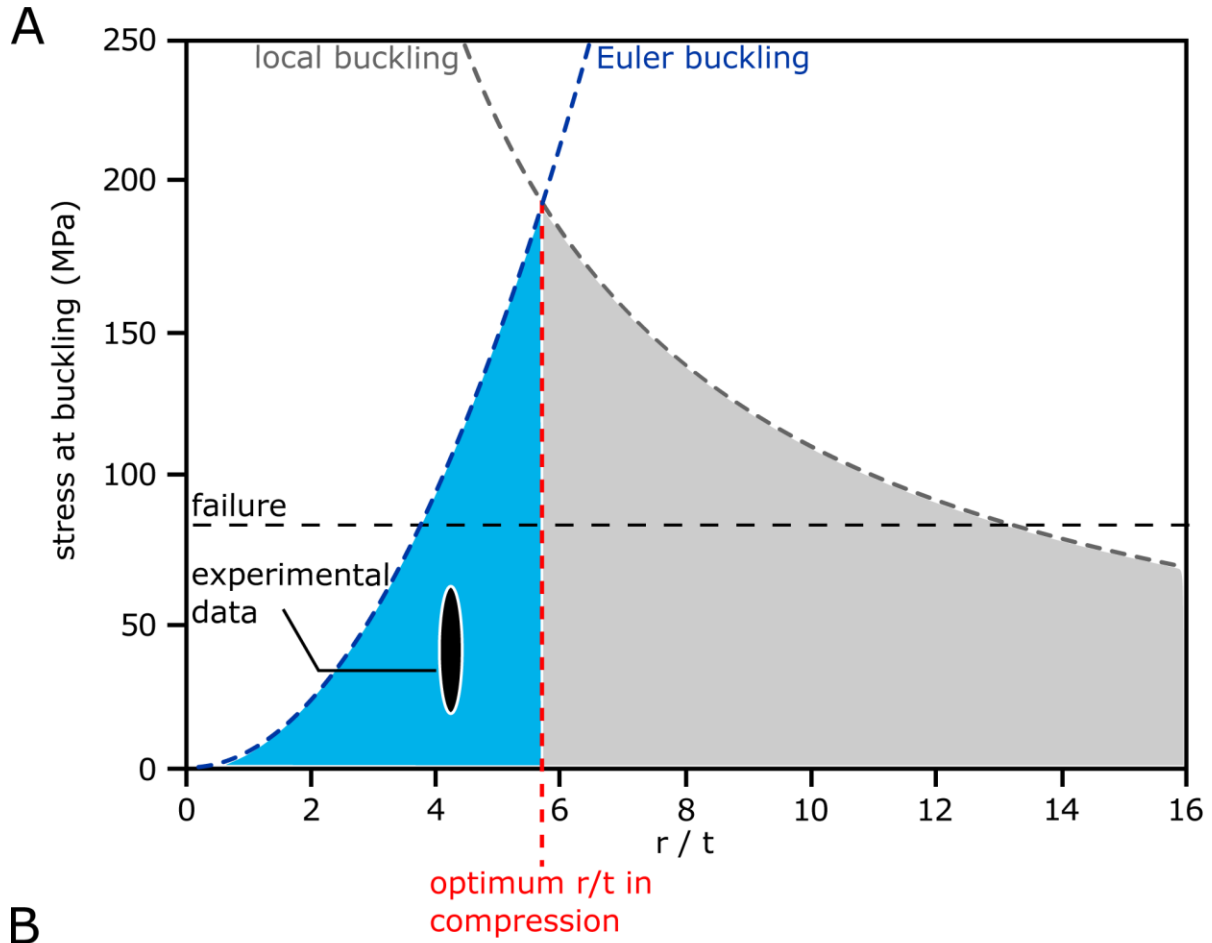
Figure 5: Theoretical prediction of the optimal radius to thickness (r/t) ratio of the hindleg tibia when loaded in compression. The comparisons are made between the theoretical and experimental data at all postembryonic developmental stages. (A) Stress at buckling versus r/t ratio for the tibia at the adult stage. The load-carrying capacity of the tibia predicted by Euler buckling (blue dash-line) and local buckling (grey dash line) is plotted as a function of r/t ratio. The optimum value of r/t occurs at the point where the two curves intersect (shown by red dash-line). Assuming a yield strength of about 85 MPa (Parle et al., 2015), the horizontal black dash-line gives the stress in which the tibia cuticle may fail due to plasticity. The experimental data obtained from measurements on tibiae of adult stick insects lie within the black ellipse. (B) Comparison of the theoretically predicted optimal (red) and experimentally measured (black) r/t values at each developmental stage. Except at the fifth nymphal stage (L5), the experimental r/t values are close to the optimum value.

Table 1. Results of mechanical and geometric measurements at each developmental stage. The data are shown as mean ± standard deviation.

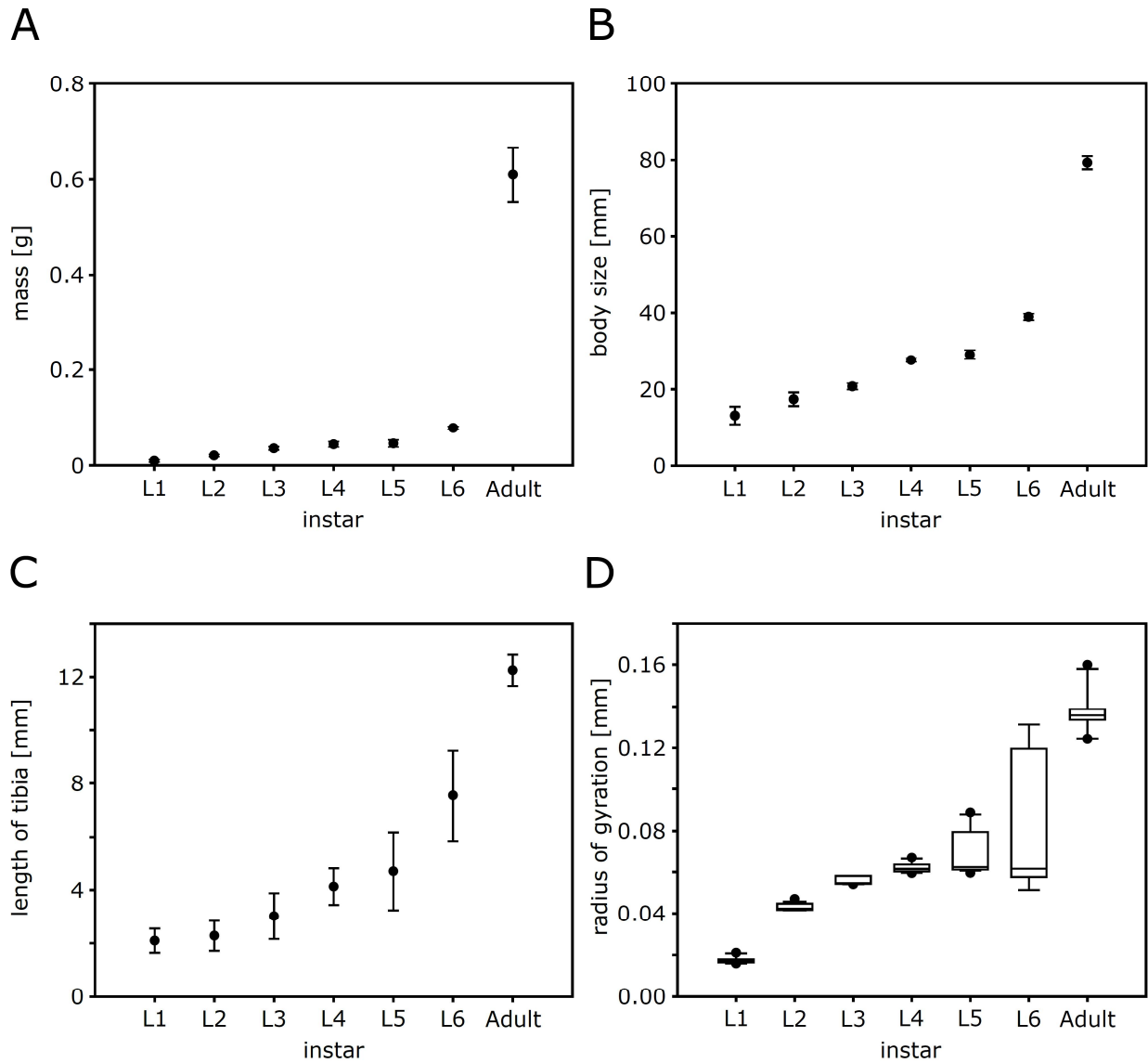| developmental stage	number of tibia specimens	critical force [mN]	stress at buckling [MPa]	effective Young's modulus [GPa]	slenderness ratio	radius to thickness ratio	area ratio of hard to soft cuticle
L1	10	4.4±2.1	66.7±14.2	1.18±0.28	67.7±11.4	6.84±0.67	0.39±0.03
L2	14	13.8±8.4	39.5±14.0	0.80±0.26	52.7±13.3	8.10±0.65	0.34±0.02
L3	11	32.2±12.1	49.3±18.7	1.46±0.71	52.4±14.6	9.51±0.79	0.44±0.03
L4	11	38.6±21.6	45.5±22.5	1.79±1.03	66.5±11.5	9.16±1.35	0.46±0.05
L5	17	75.7±25.6	67.3±23.6	2.84±0.59	66.0±11.1	13.13±1.21	0.54±0.03
L6	10	93.2±28.8	65.6±24.2	4.46±0.58	101.8±28.3	4.32±0.41	0.65±0.01
Adult	16	126.8±19.9	37.4±15.9	3.65±0.79	106.7±15.9	4.23±0.24	0.57±0.03

Figure S1: Changes of (A) body mass, (B) body size, (C) length of the tibia and (D) radius of gyration of the tibia at all postembryonic developmental stages of the stick insect *C. morosus*.

Video S1: The onset and evolution of local buckling in a tibia specimen at the fifth nymphal stage (L5).

Video S2: The onset and evolution of Euler buckling in a tibia specimen at the adult stage.